Absorption Spectra of Several Metal Complexes Revisited by the Time-Dependent Density-Functional Theory-Response Theory Formalism

P. Boulet,[†,‡] H. Chermette,[*,‡] C. Daul,[§,#] F. Gilardoni,[||] F. Rogemond,[⊥] J. Weber,[†] and G. Zuber[§]

Université de Genève, Département de Chimie Physique, 30 quai E-Ansermet, CH-1211 Genève 4, Suisse, Université Claude Bernard Lyon 1, Laboratoire de Chimie-Physique Théorique, Bât 201, 43 Bd du 11 novembre 1918, 69622 Villeurbanne Cedex, France and Institut de Recherches sur la Catalyse, UPR 5401, 69626 Villeurbanne Cedex, France, Institut de Chimie Inorganique, Université de Fribourg, Pérolles, CH-1700 Fribourg, Suisse, Department of Chemical Engineering, UCB Berkeley, 210-A Gilman Hall, California 94720-1462, Université Jean Monnet, Laboratoire Traitement du Signal et Instrumentation, 34 rue du Docteur Paul Michelon, 42023 Saint-Etienne Cedex 2, France

Received: August 23, 2000; In Final Form: November 15, 2000

Vertical excitations calculated for the CrO_4^{2-}, MnO_4^-, RuO_4, CrF_6, $FeCp_2$, $RuCp_2$ and CpNiNO species are compared to experimental spectra. The results obtained from the time-dependent density-functional theory−response theory (TD-DFRT) method are compared to both previously reported ΔSCF calculations and experiment. The results show that, in general, excited states of metal oxide and metallocene compounds are well described by TD-DFRT. However, serious difficulties are met with the CrF_6 system.

I. Introduction

Since the pioneering work of Slater, almost five decades ago, with the well-known Xα exchange functional,[1] density functional theory (DFT) has been constantly developed and our knowledge of the physical principles underlying this theory[2] has been deeply increased. DFT is now one of the most widely used methodologies to deal with quantum description of chemical systems. However, up to now, within the Kohn−Sham formalism,[3] DFT was suffering from intrinsic troubles termed "the bad asymptotic behavior of the exchange-correlation potential" and "the generalization of the Hohenberg and Kohn theorems to excited states". If calculations of optical spectra of chemical systems were tractable, under certain conditions, thanks to the early works of Slater,[4] Ziegler et al.,[5] and Daul,[6] an accurate description of dispersion forces such as van der Waals forces (closely related to the behavior of the exchange-correlation potential) has not yet been achieved. To overcome these problems, considerable work has been done over the past decade and, for instance, time-dependent density-functional response theory (TD-DFRT) has now become a comprehensive and practical methodology to deal with those physical problems (see refs 7−10 for a more rigorous reformulation of the action principle).

To treat time-dependent chemical phenomena, one has to solve the corresponding time-dependent Schrödinger equation:

$$\hat{H}(\mathbf{r},t)\Psi(\mathbf{r},t) = i\frac{\partial}{\partial t}\Psi(\mathbf{r},t) \tag{1}$$

with $\hat{H} = \hat{T} + U + V(t)$, where T is the kinetic energy operator, U is the electron−electron potential and $V(t)$ is a time-dependent external potential.

According to the variational action principle one can derive a set of time-dependent Kohn−Sham-like equations:

$$\left\{-\frac{1}{2}\nabla_i^2 + v_{\text{eff}}(\mathbf{r},t)\right\}\Phi_i(\mathbf{r},t) = i\frac{\partial}{\partial t}\Phi_i(\mathbf{r},t) \tag{2}$$

where

$$v_{\text{eff}}(\mathbf{r},t) = v(\mathbf{r},\mathbf{t}) + \int\frac{\rho(\mathbf{r},t)}{|\mathbf{r}-\mathbf{r}'|}d\mathbf{r}' + v_{\text{xc}}(\mathbf{r},t) \tag{3}$$

$v(\mathbf{r},t)$ being the nuclear potential, the integral term being the classical coulomb repulsion potential, and $v_{\text{xc}}(\mathbf{r},t)$ being the time-dependent exchange-correlation potential. Here, $v_{\text{xc}}(\mathbf{r},t)$ is defined by

$$v_{\text{xc}}(\mathbf{r},t) = \frac{\delta A_{\text{xc}}[\rho]}{\delta\rho(\mathbf{r},t)} \tag{4}$$

where $A_{\text{xc}}[\rho]$ is the universal exchange-correlation action functional.

Whereas this functional is still unknown, it can be approximated within the adiabatic approximation by the commonly used exchange-correlation functionals $E_{\text{xc}}[\rho_t]$, which are only dependent on the density $\rho_t(\mathbf{r})$ of the system at the instant t. Hence,

$$v_{\text{xc}}(\mathbf{r},t) \approx \frac{\delta E_{\text{xc}}[\rho_t]}{\delta\rho_t(\mathbf{r})} = v_{\text{xc}}[\rho_t] \tag{5}$$

The time-dependent perturbation potential $v_{\text{eff}}(\mathbf{r},t)$, periodic with ω, induces a variation of the density $\delta\rho(\mathbf{r},t)$ that can be expressed as a function of the linear response of the Kohn−Sham density matrix $\delta P(\omega)$, which in turn depends on a

* To whom correspondence should be addressed: cherm@catalyse.univ-lyon1.fr
[†] Université de Genève.
[‡] Université Claude Bernard Lyon 1.
[§] Université de Fribourg
[||] UCB Berkeley.
[⊥] Université Jean Monnet.
[#] Claude.Daul@unifr.ch

10.1021/jp003041q CCC: $20.00
Published on Web 01/17/2001

coupling matrix *K*. This matrix stands for the linear response of the Coulomb and exchange-correlation potentials. The complete neglect of the coupling matrix is called the IP (independent particule) approximation.[11] If only the Coulomb potential response is accounted for, the procedure is denoted as the RPA (for random phase approximation). The accuracy of these methods together with that of the fully coupled adiabatic approximation (where the response of the exchange-correlation potential is also accounted for) has been compared on the basis of the polarizability property and the optical spectrum of N_2.[11]

Finally, as the perturbative time-dependent potential has the form of an electric field the mean dynamic polarizability $\bar{\alpha}(\omega)$ can be derived from the real part of $\delta P(\omega)$

$$\bar{\alpha}(\omega) = \frac{1}{3} Tr\alpha(\omega) = \sum_I \frac{f_I}{\omega_I^2 - \omega^2} \qquad (6)$$

where the poles $\omega_I = E_I - E_0$ and the residues f_I turn out to be the vertical excitation energies and the oscillator strength, respectively.

To date, the accuracy of TD-DFRT has been tested on an increasing number of small molecules of organic interest such as N_2, H_2CO, CH_4, C_2H_4, pyridine, free-base porphine, and benzene, for which excitation energies,[11] static and dynamic polarizabilities,[12] hyperpolarizabilities and van der Waals dispersion coefficients[13] and Raman scattering intensities[14] have been investigated.

To our knowledge only two theoretical works[15,16] on optical spectra of transition metal complex systems has been published using the TD-DFRT formalism. The purpose of this article is to present calculations of the optical absorption of the CrO_4^{2-}, MnO_4^-, RuO_4, CrF_6, $FeCp_2$, $RuCp_2$, and CpNiNO complexes.

For a large subset of compounds and for sake of comparison, the transition energies calculated using the ΔSCF method by one of us[30] have been reported. This method, well documented elsewhere,[5,6] provides a reasonable estimation of the transition energies. The corresponding intensities were not calculated.

II. Computational Approach

Most of the calculations have been performed within the TD-DFRT formalism as implemented in ADF99.[17−19]

As far as the CpNiNO complex is concerned, transition energies have been calculated using the Davidson algorithm, which enables us to choose a restricted set of excitations corresponding to the symmetry of the excited state. Therefore, only the transition energies from the $^1A_1$ ground state to the $^1A_1$ and $^1E_1$ excited states have been calculated because transitions to other state symmetries are forbidden by selection rules.

The structure of the CpNiNO complex has been calculated at the LDA (local density approximation) level using the VWN correlation functional.[20] With this structure, TD-DFRT calculations have been performed at the LDA and GGA (generalized gradient approximation) levels using the B88P86 potential,[21,22] and the asymptotically well-behaved LB94[23] and LRC[24] potential functionals. The corresponding results will be referred to as LDA//LDA, B88P86//LDA, LB94//LDA, and LRC//LDA, respectively. Furthermore, the CpNiNO complex has been optimized using the B88P86 functional. TD-DFRT results corresponding to this geometry will be referred to as B88P86//B88P86, LB94//B88P86, and LRC//B88P86, respectively. At this stage of the description it is essential to emphasize that regardless of the potential used during the SCF procedure, the coupling matrix used to evaluate response properties belongs to the adiabatic local density approximation.

TABLE 1: Experimental and Calculated Metal-to-Ligand Bond Lengths of the d^0−Metal Complexes[a]

	LDA	B88P86	PW91	B3LYP	exp
CrO_4^{2-}					
r_{Cr-O} (pm)	166.1	168.3	168.1	166.7	166.0[31]
MnO_4^-					
r_{Mn-O} (pm)	160.7	162.8	162.6	161.3	161.0−163.0[37,38]
RuO_4					
r_{Ru-O} (pm)	171.2	173.2	173.0	173.5	166.0−185.0[42]
CrF_6					
r_{Cr-F} (pm)	173.2	176.0	176.0		
$FeCp_2$					
r_{Fe-Cp} (pm)	163.7	169.3	168.9		166.0[56]
$RuCp_2$					
r_{Ru-Cp} (pm)	181.0	185.9	185.6		181.6[47]

[a] For metallocenes, r*M*−*Cp* stands for the vertical distance.

The valence basis sets used for all atoms are a combination of three Slater-type orbitals with the addition of a polarization function on C, N, O, and H atoms, whereas frozen core potentials have been used to model inner electrons. Finally, the level of accuracy has been chosen to be 5 (according to ADF convention) for the computation of numerical integrations.

For the remaining complexes, the geometries have been optimized using the VWN, the B88P86, and the PW91 (exchange and correlation) functionals.[25] The quality of the basis set is the same as for the CpNiNO complex. For each geometry, an excited states calculation has been performed using the asymptotically well-behaved LB94 functional. Finally, the B3LYP[26] functional has been tested within the Gaussian 98 program package,[27] both for the geometry and the excited states calculations. In this case, the LAND2DZ basis set[28] has been used.

III. Excited States of Metal Oxide Compounds

A. The Chromate Ion. The chromate anion CrO_4^{2-} has an intense yellow color. Its symmetry is T_d and the formal oxidation state of the metal is Cr(VI). Hence, its formal electron configuration is d^0. Thus, we essentially expect LMCT (ligand to metal charge transfer) transitions.

The first theoretical study of the CrO_4^{2-} excited states has been reported by Wolfsberg and Helmholz[29] in 1952 using a molecular orbital treatment parametrized with the famous Wolfsberg−Helmholz formula. Although the predicted energy bands were slightly downshifted compared to experiments, the authors could correctly assign the 3.36 eV energy band to a $^1T_2 \leftarrow {}^1A_1(1t_1 \rightarrow 2e)$ transition and the 4.61 eV energy band to a $^1T_2 \leftarrow {}^1A_1(4t_2 \rightarrow 2e)$ one, which was a real challenge at this time. More recently, Stückl et al. have reinvestigated the absorption spectrum of this complex using both the Slater's transition state method and the ΔSCF method.[30]

1. Geometry Optimization of CrO_4^{2-}. The geometry of the CrO_4^{2-} anion has been optimized using the four different functionals previously mentioned retaining the T_d symmetry. Table 1 reports the metal−ligand bond distances. It is interesting to notice that both LDA and B3LYP yield the correct bond length and GGA does slightly overestimate it by roughly 2.0 pm.

2. Transition Energies of CrO_4^{2-}. Figure 1 presents the absorption spectrum of the chromate ion CrO_4^{2-} in an aqueous solution of potassium chromate.[31] We observe two main bands at 3.36 and 4.61 eV. These two bands are associated with an LMCT transition from occupied ligand orbital to empty one on

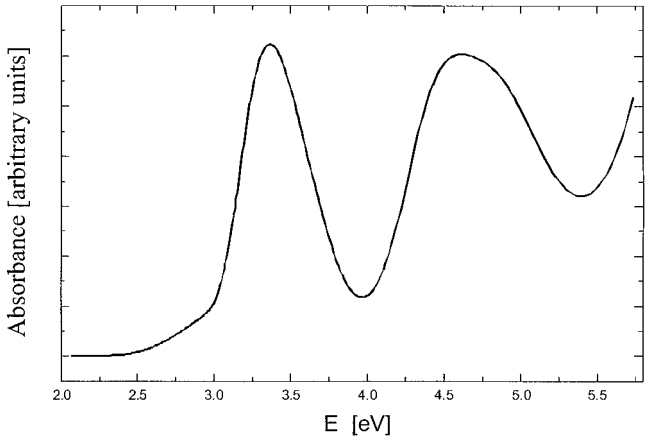

Figure 1. Absorption spectrum of K_2CrO_4 (aq.)

the metal. On the basis of our calculations, it is possible to assign the first band to a charge transfer $1t_1 \rightarrow 2e(^1T_2)$ from a π type molecular orbital on the ligands to an empty d orbital of the metal (Table 2).

The second band, however, results from two LMCT transitions i.e., $4t_2 \rightarrow 2e(^1T_2)$ and $1t_1 \rightarrow 5t_2$ ($^1T_2$). Moreover, one notices also on Figure 1 a shoulder between 2.5 and 3.0 eV which is probably due to an electric dipole forbidden. According to our calculations (see Table 2), this transition is associated to the $1t_1 \rightarrow 2e(^1T_1)$ one.

In the scheme below, we list the states arising within the LMCT manifold. The state in boldface $^1A_1 \rightarrow {}^1T_2$ is electric dipole allowed.

$$(4t_2)^6(1t_1)^6 \rightarrow (4t_2)^6(1t_1)^5(2e),\ E \otimes T_1 = {}^3T_1 + {}^3T_2 + {}^1T_1 + \mathbf{{}^1T_2}$$

$$(4t_2)^6(1t_1)^6 \rightarrow (4t_2)^5(1t_1)^6(2e),\ E \otimes T_2 = {}^3T_1 + {}^3T_2 + {}^1T_1 + \mathbf{{}^1T_2}$$

$$(4t_2)^6(1t_1)^6 \rightarrow (4t_2)^6(1t_1)^5(5t_2),\ T_2 \otimes T_1 = {}^3T_1 + {}^3T_2 + {}^1T_1 + \mathbf{{}^1T_2} + {}^3A_2 + {}^3E + {}^1A_2 + {}^1E$$

The agreement between experiment[31] and calculations is good. In particular, we emphasize the excellent predictions obtained when using the LB94 potential functional. The results obtained with the different methods are slightly scattered, but the statistical significance of the prediction is comparable to the experimental accuracy of room temperature solution spectra. It is remarkable that the combination of a GGA geometry with the LB94 functional always decreases the transition energies compared to the LB94//LDA results. Furthermore, one can notice that the LB94//B88P86 and the LB94//PW91 procedures lead to the same results both for transition energies and intensities. The ΔSCF procedure gives relatively satisfactory transition energies, though overestimated, compared to all other results. This is probably related to the LDA potential which is known to give only a small number of bonded virtual orbitals. This trend is corrected by an asymptotically well-behaved potential such as LB94. Until now, few potentials have been proposed which respect the $-1/r$ asymptotics. As examples, the well-known HCTH(AC) potential of Tozer et al.,[32,33] the SAOP potential of Gritsenko et al.,[34] and the potential used by Casida et al.[35] significantly improve excitation energies toward Rydberg states.

B. The Permanganate Ion. The second member of our series of d^0 metal ions is the permanganate anion MnO_4^-. In this case, manganese is in a +VII oxidation state. Hence, we expect the same spectroscopical features as for the CrO_4^- compound. The experimental spectrum of the MnO_4^- complex has also been interpreted by Wolfsberg and Helmholz.[29] Later, Holt and Ballhausen[36] did experimentally reinvestigate the absorption spectrum which features four bands centered at 2.3, 3.5, 4.0, and 5.5 eV. Among these peaks, both the first and the third peaks exhibit strong vibronic structures.

1. Geometry Optimization of MnO_4^-. The structure of the MnO_4^- complex has been obtained from X-ray diffraction data of solid potassium permanganate.[37,38] According to these experimental results, the manganese atom is surrounded by four oxygen atoms roughly located at the corners of a regular tetrahedron. As before, the geometry of the MnO_4^- anion has been optimized with both same functionals and basis sets within T_d symmetry. As already mentioned, the calculated metal-to-ligand bond lengths are within the usual confidence limit of $\pm$2.0 pm (see Table 1). As the LDA and B3LYP bond lengths are slightly too short, it is not surprising that GGA functionals lead to better results.

2. Transition Energies of MnO_4^-. The main features of the permanganate ion spectrum[36] are similar to those observed previously for chromate, the major difference being the observation in the 2−6 eV region and at room temperature of vibrational structure,[36,39] (ν = 750 cm^{-1}), which corresponds to a totally symmetric stretch of the Mn−O bonds for the first optical transition located at 2.19 eV (0−0 transition) and the third one located at 3.76 eV (0−0 transition).

The first band can be assigned to a singlet state $^1T_2(1t_1 \rightarrow 2e)$, which originates from a ligand to metal charge transfer. The three remaining bands at 3.50 eV ($4t_2 \rightarrow 2e$, $^1T_2$), 3.76 eV ($1t_1 \rightarrow 5t_2$, $^1T_2$) (0−0, max. 4.00 eV), and 5.51 eV ($5a_1 + 3t_2 \rightarrow 5t_2$, $^1T_2$) are also due to a charge transfer from ligands to metal. It should be mentioned that in the case of $t_1 \rightarrow t_2$ excitations, symmetry considerations alone are not sufficient to discriminate between $^1T_1$ and $^1T_2$ states energies. Therefore, within the sum method, the $^1T_1$ and $^1T_2$ states have the same averaged energy. However, it has been shown[40] that the calculation of some two-electron integrals can override this problem (see below).

The five observed spin and symmetry-allowed transitions originate from the five configurations listed below. The transitions to the state in boldface $^1A_1 \rightarrow {}^1T_2$ are the only electric dipole allowed ones and hence carry most of the intensity.

$$(4t_2)^6(1t_1)^6 \rightarrow (4t_2)^6(1t_1)^5(2e),\ E \otimes T_1 = {}^3T_1 + {}^3T_2 + {}^1T_1 + \mathbf{{}^1T_2}$$

$$(4t_2)^6(1t_1)^6 \rightarrow (4t_2)^5(1t_1)^6(2e),\ E \otimes T_2 = {}^3T_1 + {}^3T_2 + {}^1T_1 + \mathbf{{}^1T_2}$$

$$(4t_2)^6(1t_1)^6 \rightarrow (4t_2)^6(1t_1)^5(5t_2),\ T_2 \otimes T_1 = {}^3T_1 + {}^3T_2 + {}^1T_1 + \mathbf{{}^1T_2} + {}^3A_2 + {}^3E + {}^1A_2 + {}^1E$$

$$(4t_2)^6(1t_1)^6 \rightarrow (4t_2)^5(1t_1)^6(5t_2),\ T_2 \otimes T_2 = {}^3T_1 + {}^3T_2 + {}^1T_1 + \mathbf{{}^1T_2} + {}^3A_1 + {}^3E + {}^1A_1 + {}^1E$$

$$(3a_1)^2(4t_2)^6(1t_1)^6 \rightarrow (3a_1)(4t_2)^6(1t_1)^6(5t_2),\ A_1 \otimes T_1 = {}^3T_2 + \mathbf{{}^1T_2}$$

Results are given in Table 2. As for the first and the third transition, vibration structure is observed. Both the maximum

TABLE 2: Lowest Electronic Transitions (eV) of the d^0−Metal Complexes[a]

		ΔSCF(LDA)[30]	LB94//LDA	LB94//B88P86	LRC//B88P86	LB94//PW91	B3LYP	exp
CrO_4^{2-}								
$^1T_1$	$1t_1 \rightarrow 2e$		2.988 (0.0000)	2.835 (0.0000)	2.852 (0.0000)	2.849 (0.0000)	3.146	2.75[31]
$^1T_2$	$1t_1 \rightarrow 2e$	3.62	3.361 (0.0282)	3.199 (0.0256)	3.211 (0.0094)	3.214 (0.0258)	3.604	3.36[31]
$^1T_2$	$4t_2 \rightarrow 2e$		4.279 (0.0124)	4.086 (0.0105)	4.119 (0.0032)	4.104 (0.0107)	4.599	4.61[31]
$^1T_2$	$1t_1 \rightarrow 5e_2$		5.149 (0.0222)	4.919 (0.0222)	4.915 (0.0067)	4.939 (0.0222)	4.942	
MnO_4^-								
$^1T_2$	$1t_1 \rightarrow 2e$	2.70	2.757 (0.0184)	2.628 (0.0167)	2.631 (0.0062)	2.825 (0.0209)	2.805	2.3 (2.19, 0→0)[36]
$^1T_2$	$4t_2 \rightarrow 2e$	4.01	3.772 (0.0074)	3.602 (0.0061)	3.634 (0.0019)	3.899 (0.0027)	3.876	3.7[36]
$^1T_2$	$1t_1 \rightarrow 5t_2$	4.26	4.722 (0.0219)	4.516 (0.0209)	4.519 (0.0070)	4.756 (0.0285)	4.414	4.0 (3.76, 0→0)[36]
$^1T_2$	$5a_1 + 4t_2 \rightarrow 5t_2$	5.69	5.695 (0.0053)	5.472 (0.0069)	5.496 (0.0005)	5.865 (0.0119)		5.5[31]
RuO_4								
$^1T_2$	$1t_1 \rightarrow 2e$	3.33	3.186 (0.0126)	3.035 (0.0117)	3.087 (0.0047)	3.050 (0.0118)	2.929	3.22[43]
$^1T_2$	$4t_2 \rightarrow 2e$		3.975 (0.0255)	3.802 (0.0220)	3.854 (0.0075)	3.819 (0.0224)	3.854	4.00[43]
$^1T_2$	$5a_1 + 4t_2 \rightarrow 5t_2$		5.248 (0.0115)	5.009 (0.0113)	5.045 (0.0039)	5.033 (0.0113)	4.692	4.96[43]

[a] The values in parentheses are the oscillators strengths.

of the Franck−Condon envelop and the electronic origin of the bands are indicated. It is worth noting that, independently from the method of calculation, the agreement between the observations and the predictions is slightly less satisfatory in the case of the permanganate than for chromate. Roughly speaking, the predicted energies are between 0.1 and 0.5 eV too high depending on the method considered. Contrarily to previous results obtained for the CrO_4^{2-} complex, the PW91 geometry gives sytematically higher transition energies when TD-DFRT is applied, compared to the LDA and B88P86 ones. Moreover, the LB94//B88P86 and the LB94//PW91 functionals give significantly different results. This is also obvious when one compares the oscillator strengths. The transition energies are overestimated by the latter functionals, thus worsening the results by about 0.2 eV compared to the LB94//B88P86 procedure. Finally, as for the CrO_4^{2-} complex, the ΔSCF method[30] yields overestimated transition energies compared to experiment.

A pertinent study of MnO_4^- splitting multiplets has been performed by Dickson and Ziegler.[41] By computing some selected two-electron integrals, they could calculate the energies of the $^1T_1$ and $^1T_2$ states arising from the $1t_1 \rightarrow 5t_2$ transition. The main interesting feature is the crossing between two $^1T_2$ states, namely the one just mentioned and the one arising from the $4t_2 \rightarrow 2e$ excitation (see Table 2). Consequently, the ordering of the states obtained from TD-DFT calculations is no longer in agreement with that obtained by Dickson and Ziegler.

Recently, van Gisbergen et al. reported a study bearing on excitation energies of several metal compounds including the MnO_4^- complex.[16] As they have used the LB94//LDA procedure (denoted as LB94/ALDA in their paper) in conjunction to a diffuse basis set, we can investigate the effect of adding diffuse functions to the basis set on excitation energies. Whatever the transition considered, the effect of diffuse functions is to lower the excitation energies by at least 0.1 eV. It is remarkable that the highest lying state ($^1T_2(5a_1 + 4t_2 \rightarrow 5t_2)$) is lowered by 0.23 eV leading to a very good estimate of the transition energy (ca. 5.46 eV compared to exp. 5.50 eV). The fact that the addition of diffuse functions to the basis set improves the prediction of high-lying state energies is related to the anionic character of the studied complexes. The necessity of using diffuse functions, not necessarily important for the ground-state description, both enhances the description of the excited-state density of the anion and its density response function.

C. The Ruthenium Oxide Complex. This is the last member of our series of d^0 metal complexes. The main difference with the two previous ones is that it is neutral, the metal has a maximum oxidation state of +VIII and 4d orbitals instead of 3d ones are involved.

1. Geometry Optimization of RuO_4. The experimental values of the Ru−O bond lengths were determined by IR spectroscopy in gas phase.[42] By analogy with the OsO_4 complex it was suggested that the ruthenium oxide would be tetrahedral. The IR study leaves little doubt on this assumption. However, X-ray diffraction and electron diffraction spectroscopies yielded large discrepancies on the Ru−O bond length (179.0 pm and 166.0 pm according to X-ray diffraction and electron diffraction experiments, respectively). The results are presented in Table 1. It should be mentioned that the Os−O bond length in the OsO_4 complex is estimated to amount to 166.0 pm.

As expected, all calculated bond distances are within the experimental error bars. However, if we consider the 179.0 pm as being the best estimates for the bond distance, it is noticeable that whatever the functional used, calculated bond lengths are too short by about 7.0 pm.

2. Transition Energies of RuO_4. In Table 2 we compare the experimental transition energies of the low-lying optical transitions of ruthenium tetroxide observed by UV/vis spectroscopy[43] with the transition energies obtained by calculations. Overall, the agreement between the experimental observations and the predictions is excellent. From a theoretical point of view, results obtained for the RuO_4 complex are basically similar to that obtained for the CrO_4^{2-} complex: the LB94//B88P86 and the LB94//PW91 procedures predict both the same transition energies and intensities, and the maximum deviation amounts to about 0.3 eV. On the contrary, it is noteworthy that the B3LYP functional gives quite an unsatisfactory description of the first peak, which is much too high (0.7 eV). Finally, as for the previous anion complexes, the ΔSCF[30] slightly overestimates the excitation energy of the $^1T_2 \leftarrow {}^1A_1(1t_1 \rightarrow 2e)$ transition by only 0.11 eV.

D. Conclusion on Metal Oxide Complexes. Briefly, we can emphasize that the TD-DFRT formalism is adequate to reproduce excitation energies of metal oxide complexes. Compared to the ΔSCF method, it generally lowers the transition energies by a few tenths of electron-volts, therefore improving the description of the whole spectrum. In the case of the MnO_4^- complex, however, TD-DFRT seems to meet some difficulties. The fact that the MnO_4^- complex is an anion is probably not the main reason of this behavior because we observe that the spectrum of the CrO_4^{2-} complex is, on the contrary, both rather insensitive to the addition of these diffuse functions and well reproduced (data not reported in Table 2).

TABLE 3: Observed and Calculated Excitation Energies (eV) of the LMCT Transitions of the Hexafluoro-chromium(VI)

		LB94//LDA	LB94//B88P86	LRC//B88P86	LB94//PW91	B3LYP	exp[44]
$^1T_{1u}$	$(3t_{1u} + 1t_{2u}) \rightarrow 2t_{2g}$	2.38 (0.0002)	2.22 (0.0001)	2.27 (0.0002)	2.22/0.0002	2.30	3.31
$^1T_{1u}$	$(2t_{1u} + 1t_{2u} + 3t_{1u}) \rightarrow 2t_{2g}$	3.12 (0.0138)	2.96 (0.0129)	2.98 (0.0143)	2.96/0.0129	3.21	3.87
$^1T_{1u}$	$(2t_{1u} + 1t_{2u} + 3t_{1u}) \rightarrow (2t_{2g} + 3e_g)$	4.21 (0.0406)	3.98 (0.0356)	4.04 (0.0394)	3.98/0.0356	4.18	4.77

IV. Excited States of the Hexafluoro-Chromium(IV) Metal Halide Compounds

The CrF_6 complex is neutral and thus has a d^0 electronic configuration. Hence, one essentially does expect LMCT transitions. The geometry has been optimized. The complex has octahedral O_h symmetry. The valence electronic structure of this compound is

$$3t_{1u}^6(F_{p_x p_y p_z}) < 1t_{2u}^6(F_{p_x p_y p_z}) < 4t_{1u}^6(F_{p_x p_y p_z}) < 1t_{1g}^6(F_{p_y p_z}) \ll 2t_{2g}^0(d_{xy},d_{yz},d_{xz}) \ll 3e_g^0(d_{x^2-y^2},d_{z^2})$$

With this LMCT manifold, the following set of multiplets is expected:

$$(3t_{1u})^6(1t_{2u})^6(4t_{1u})^6(1t_{1g})^6 \rightarrow (3t_{1u})^6(1t_{2u})^6(4t_{1u})^6(1t_{1g})^5(2t_{2g}),\ T_{1g} \otimes T_{2g} = {}^{3,1}A_{2g} + {}^{3,1}E_g + {}^{3,1}T_{1g} + {}^{3,1}T_{2g}$$

$$(3t_{1u})^6(1t_{2u})^6(4t_{1u})^6(1t_{1g})^6 \rightarrow (3t_{1u})^6(1t_{2u})^6(4t_{1u})^6(1t_{1g})^5(3e_g),\ T_{1g} \otimes E_g = {}^{3,1}T_{1g} + {}^{3,1}T_{2g}$$

$$(3t_{1u})^6(1t_{2u})^6(4t_{1u})^6(1t_{1g})^6 \rightarrow (3t_{1u})^6(1t_{2u})^6(4t_{1u})^5(1t_{1g})^6(2t_{2g}),\ T_{1u} \otimes T_{2g} = {}^{3,1}A_{2u} + {}^{3,1}E_u + {}^{3,1}\boldsymbol{T_{1u}} + {}^{3,1}T_{2u}$$

$$(3t_{1u})^6(1t_{2u})^6(4t_{1u})^6(1t_{1g})^6 \rightarrow (3t_{1u})^6(1t_{2u})^6(4t_{1u})^5(1t_{1g})^6(3e_g),\ T_{1u} \otimes E_g = {}^{3,1}\boldsymbol{T_{1u}} + {}^{3,1}T_{2u}$$

$$(3t_{1u})^6(1t_{2u})^6(4t_{1u})^6(1t_{1g})^6 \rightarrow (3t_{1u})^6(1t_{2u})^5(4t_{1u})^6(1t_{1g})^6(2t_{2g}),\ T_{2u} \otimes T_{2g} = {}^{3,1}A_{1u} + {}^{3,1}E_u + {}^{3,1}\boldsymbol{T_{1u}} + {}^{3,1}T_{2u}$$

$$(3t_{1u})^6(1t_{2u})^6(4t_{1u})^6(1t_{1g})^6 \rightarrow (3t_{1u})^6(1t_{2u})^5(4t_{1u})^6(1t_{1g})^6(3e_g),\ T_{2u} \otimes E_g = {}^{3,1}\boldsymbol{T_{1u}} + {}^{3,1}T_{2u}$$

$$(3t_{1u})^6(1t_{2u})^6(4t_{1u})^6(1t_{1g})^6 \rightarrow (3t_{1u})^5(1t_{2u})^6(4t_{1u})^6(1t_{1g})^6(2t_{2g}),\ T_{1u} \otimes T_{2g} = {}^{3,1}A_{2u} + {}^{3,1}E_u + {}^{3,1}\boldsymbol{T_{1u}} + {}^{3,1}T_{2u}$$

$$(3t_{1u})^6(1t_{2u})^6(4t_{1u})^6(1t_{1g})^6 \rightarrow (3t_{1u})^5(1t_{2u})^6(4t_{1u})^6(1t_{1g})^6(3e_g),\ T_{1u} \otimes E_g = {}^{3,1}\boldsymbol{T_{1u}} + {}^{3,1}T_{2u}$$

Hope and co-workers[44] have reported experimental IR and UV spectra of chromium fluorides such as CrF_4, CrF_5, and CrF_6. Experiments were performed both in solid state and in argon matrix isolation. We report in Table 3 results obtained from matrix isolation experiments.

The spectrum of the CrF_6 complex features three bands located at 3.31, 3.87, and 4.76 eV. Experimentalists assign these peaks to LMCT's. More precisely, both, the $3t_{1u}^6$ and the $4t_{1u}^6$ molecular orbitals and the $1t_{2u}^6$ molecular orbital are 100% of ligand character, whereas the LUMO $2t_{2g}^0$ exhibits 65% of chromium character and 35% of ligand character.

According to the selection rules for octahedral complexes, only the $^1T_{1u} \leftarrow {}^1A_{1g}$ transitions are both spin and symmetry allowed. Table 3 shows the results of our excitation energy calculations. The LB94//B88P86, LB94//PW91, and the B3LYP functionals give transition energies that are much too low. It is noteworthy that both the LB94//B88P86 and the LB94//PW91 results are strictly identical. This is related to the fact that both geometries are the same. For this complex, the best functional would be the LB94 one at the local geometry (LDA). However, none of the functionals used give a satisfactory description of the spectrum. The addition of diffuse functions into the basis set deteriorates the agreement between calculated and experimental transition energies. In this case, as for the MnO_4^- complex, the excitation energies are lowered by about 0.1 eV. A crucial point for the magnitude of the LMCT is the bond distance between the metal center and the ligands. As we cannot compare the calculated Cr−F bond distance to the experimental one, we cannot acertain that the GGA geometry is sufficiently accurate.

V. Excited States of Cyclic Ligands Containing Metal Complexes

A. Excited States of Ferrocene. Metallocenes have been the subject of numerous experimental and theoretical studies, be it for their photophysical or for their magnetic properties. The symmetry of these molecules is either D_{5d} or D_{5h}, depending upon if the two cyclopentadienyl cycles are respectively staggered or eclipsed. In D_{5d} symmetry, the energy ordering of the metal orbitals is as follows:

$$d_{z^2}(a_{1g},\sigma) \approx d_{x^2-y^2},d_{xy}(e_{2g},\delta) \ll d_{xz},d_{yz}(e_{1g},\pi)$$

In the case of ferrocene, the metal ion has a d^6 configuration. Thus, molecular orbitals with dominant metal character are occupied up to e_{2g}, the e_{1g} being strongly antibonding. Hence, this electronic configuration will give rise to both metal centered (MC) and LMCT transitions.

In ferrocene, the HOMO−LUMO gap is quite large (>2.0 eV), hence the complex is low spin with the nonbonding metallic orbitals $5a_{1g}$ and $3e_{2g}$ completely occupied and the antibonding $4e_{1g}$ orbital empty. With this MC manifold, the following set of multiplets is expected:

$$(5a_{1g})^2(3e_{2g})^4 \rightarrow (5a_{1g})^2(3e_{2g})^3(4e_{1g}),\ E_{2g} \otimes E_{1g} = {}^3E_{1g} + {}^1E_{1g} + {}^3E_{2g} + {}^1E_{2g}$$

$$(5a_{1g})^2(3e_{2g})^4 \rightarrow (5a_{1g})^1(3e_{2g})^4(4e_{1g}),\ A_{1g} \otimes E_{1g} = {}^3E_{1g} + {}^1E_{1g}$$

The absorption spectrum of ferrocene (Figure 2) exhibits two MC bands centered at 2.7 and 3.8 eV respectively.[45] The LMCT bands appear at higher energy (4.3 eV) and are much more intense. The first MC band at 2.7 eV is in fact composed by two d−d transitions $^1E_{1g}(5a_{1g} \rightarrow 4e_{1g}) + {}^1E_{2g}(3e_{2g} \rightarrow 4e_{1g})$,

TABLE 4: Observed and Calculated Excitation Energies (eV) of the MC Transitions of Ferrocene and Ruthenocene Complexes

		ΔSCF(LDA)[46]	LB94//LDA	LB94//B88P86	LRC//B88P86	LB94//PW91	B3LYP	exp[45]
$FeCp_2$								
$^1E_{2g}$	$3e_{2g} \rightarrow 4e_{1g}$	2.87 ($^1E_2''$)	2.975	2.561	2.35	2.41	1.74	2.98
$^1E_{1g}$	$5a_{1g} \rightarrow 4e_{1g}$		3.092	2.745	2.56	2.63	2.27	2.70
$^1E_{1g}$	$3e_{2g} \rightarrow 4e_{1g}$	3.48 ($^1E_1''$)	3.621	3.245	3.07	3.16	3.22	3.82
$^3E_{2g}$	$3e_{2g} \rightarrow 4e_{1g}$		2.304	1.890	1.87	1.92		2.34
$RuCp_2$								
$^1E_1''$	$5a_1' \rightarrow 4e_1''$	3.51	3.69	3.35	3.34	3.37		3.66
$^1E_1''$	$3e_2'' \rightarrow 4e_1''$		4.21	3.82	3.78	3.85		4.54
$^1E_2''$	$3e_2'' \rightarrow 4e_1''$	3.97	3.80	3.39	3.37	3.42		4.03
$^3E_1''$	$5a_1' \rightarrow 4e_1''$	3.33	3.34	2.99	2.99	3.01		3.22

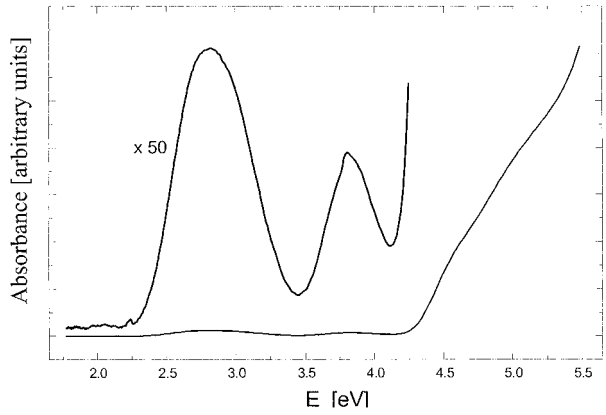

Figure 2. Absorption spectrum of ferrocene.

whereas the second band at 3.8 eV originates from a single d−d transition $^1E_{2g}(3e_{2g} \rightarrow 4e_{1g})$.

The results of our calculations are shown in Table 4. Whereas the agreement between the predicted and the observed transition energies is as expected, reasonable using TD-DFRT with GGA functionals, the results obtained with the B3LYP functional are bad, since deviations as large as 1.2 eV are observed. As for the RuO_4 complex, this is probably due to the high contribution of the HF exchange energy. The use of a GGA functional (B88P86) for the geometry optimization considerably lowers the excitation energies by at least 0.3 eV compared to the LDA results; the GGA procedure is therefore less accurate. Finally, for this complex, contrary to what is observed with other complexes, the ΔSCF excitation energies lie between that of the LB94//LDA and LB94//B88P86 procedures.

B. Excited States of the Ruthenocene Complex. Structure and UV/vis spectra of the ruthenocene complex have been experimentally investigated.[45] Also, theoretical calculations have already been performed at the ΔSCF level.[46] It was of interest, therefore, to reinvestigate this compound using the TD-DFRT approach.

1. Geometry Optimization. Contrary to the ferrocene complex, $RuCp_2$ belongs to the D_{5h} symmetry point group, therefore having eclipsed cyclopentadienyl ligands. The most important geometrical parameter is the distance between the metal center and the cycles. The results of the geometrical optimizations are depicted in Table 1. Compared to experiment,[47] the most accurate geometry is obtained using the LDA functional. The Ru−Cp bond length deviation amounts to only 0.6 pm. As a consequence, the GGA functionals with bond lengths that are too long.

2. Transition Energies of $RuCp_2$. Because of the D_{5d} symmetry, the ordering of the valence molecular orbital is slightly different from that of ferrocene:

$$d_{x^2-y^2},d_{xy}(e_2'^4,\delta) \approx d_{z^2}(a_1'^2,\sigma) \ll d_{xy},d_{yz}(e_1''^0,\pi).$$

As for the $FeCp_2$ complex, the metal center is d^6 and we expect both MC and LMCT features. We present in Table 4 only the MC transitions. The possible transitions depicted in the following scheme are very similar to that of the $FeCp_2$ complex:

$$(e_2')^4(a_1')^2(e_1'')^0 \rightarrow (e_2')^4(a_1')^1(e_1'')^1, A_1' \otimes E_1'' = {}^{3,1}E_1''$$

$$(e_2')^4(a_1')^2(e_1'')^0 \rightarrow (e_2')^3(a_1')^2(e_1'')^1, E_2' \otimes E_1'' = {}^{3,1}E_1'' + {}^{3,1}E_2''$$

The experimental UV/vis spectrum of $RuCp_2$[45] exhibits two low-intensity transitions located at 3.84 and 4.54 eV. In fact, it has been demonstrated that the first peak is composed by two transitions, the first one arising from the $5a_1' \rightarrow 4e_1''$ transition and located at 3.66 eV and the second one arising from the $3e_2'' \rightarrow 4e_1''$ transition and centered at 4.03 eV. This is in agreement with the previously proposed MC manyfold. Our calculated TD-DFRT excitation energies are gathered in Table 4. At first sight we observe that the best procedure, compared to experiment, is LB94//LDA. This is most probably due to the good geometry predicted by the local functional. Furthermore, the ΔSCF procedure gives results similar to that of LB94//LDA. On the contrary, GGA procedures poorly predict the $RuCp_2$ spectrum with a deviation amounting to at least 0.3 eV.

Finally, the spin-forbidden $^3E_1'' \leftarrow {}^1A_1'$ transition has been experimentally observed. As expected, the ΔSCF and the LB94//LDA procedures give the same value for the transition, in nice agreement with experiment. On the contrary, GGA functionals work rather poorly.

C. Excited States of the Cyclopentadienylnitrosylnickel Complex. *1. LDA versus GGA Optimized Structural Parameters.* The symmetry point group of CpNiNO is C_{5v} with a linear NiNO group of atoms. The structural parameters at LDA and GGA levels of approximation are compared to experimental parameters[48] and are reported in Table 5.

As expected, LDA bond lengths, except those involving H atoms, are shorter than GGA bond lengths. The CH bonds are slightly longer with the VWN functional, although the difference with respect to the B88P86 results amounts only to 0.3 pm.

Compared to experiment,[48] GGA results lie within the range of experimental error estimates. On the contrary, the LDA functional underestimates NiC and NiN bond lengths by 5.4 and 2.5 pm, respectively.

As the NO bond length is not reported in ref 48, its estimation from experimental data is rather inaccurate. As far as this bond is concerned, one can compare both experimental and calculated vibration frequencies for the stretching mode of NO. The B88P86 results are in a very good agreement, the discrepancy amounting to only 9 cm^{-1}. The VWN functional overestimates the vibration frequency by about 4% (25 cm^{-1}).

Finally we also report in Table 5 the ionization potentials (IP) of CpNiNO at different levels of approximations and compare them to the experimental potential.[49] As expected, the

TABLE 5: Optimized Structural Parameters and Physical Properties of the CpNiNO Complex – C_{5v} Symmetry

	LDA[b]	B88P86[b]	B88P86[49]	LB94//B88P86[b]	LRC//B88P86[b]	exp
NiC (pm)	207.6	214.3	211.8			215.0 ± 2.0[48]
NiN (pm)	160.5	162.9	163.7			165.0 ± 3.0[48]
NiO (pm)	277.2	281.0	281.5			278.0 ± 4.0[48]
NO (pm)	116.7	118.1	117.8			113.0 ± 7.0
CH (pm)	108.9	108.6	108.8			
NO stretching (cm^{-1})	1899	1815	1845			1824[48]
$-\epsilon_{HOMO}$ (eV)	5.74[c]	5.57[c]		10.86[c]	10.97[c]	
IP (eV)			8.53[c]			8.33/8.56[49]

[a] Calculated with the Slater's transition state method. [b] This work. [c] This work. Calculated using the approximation IP $\approx -\epsilon_{HOMO}$.

TABLE 6: Optical Absorption of the CpNiNO Complex at the LDA Geometry

		LDA//LDA			B88P86//LDA			LB94//LDA			LRC//LDA			exp[48]	
symmetry	M. O.[a]	energy (eV)	f (a.u.)[b]	%[c]	energy (eV)	f (a.u.)[b]	%[c]	energy (eV)	f (a.u.)[b]	%[c]	energy (eV)	f (a.u.)[b]	%[c]	energy (eV)	intensity[d]
E_1	$9a_1 \rightarrow 7e_1$	3.42	0.0002	75	3.48	0.0002	75	3.33	0.0002	90	3.35	0.0002	88	2.68	w
	$3e_2 \rightarrow 7e_1$			25			25			0			0		
E_1	$3e_2 \rightarrow 7e_1$	3.77	0.0004	74	3.83	0.0004	74	3.82	0.0002	90	3.77	0.0002	86	3.22	w
	$9a_1 \rightarrow 7e_1$			26			26			0			0		
A_1	$6e_1 \rightarrow 7e_1$	4.80	0.3617	56	4.84	0.3698	56	4.46	0.3985	66	4.43	0.4006	66	4.43	s
	$5e_1 \rightarrow 7e_1$			36			36			26			28		
E_1	$6e_1 \rightarrow 10a_1$	5.90	0.0044	100	5.92	0.0040	100	6.42	0.0013	100	5.84	0.0007	100		
E_1	$3e_2 \rightarrow 4e_2$	6.19	0.0129	64	6.20	0.0167	64	6.65	0.0087	76	6.53	0.0006	86		
	$6e_1 \rightarrow 4e_2$			30			30			0			0		
	$8a_1 \rightarrow 7e_1$			0			0			18			18		
E_1	$6e_1 \rightarrow 4e_2$	6.41	0.0558	54	6.42	0.0555	54	6.16	0.0311	56	6.12	0.0431	62	6.20	s
	$3e_2 \rightarrow 4e_2$			30			30			0			0		
	$8a_1 \rightarrow 7e_1$			0			0			41			32		
A_1	$9a_1 \rightarrow 10a_1$	6.41	0.0227	92	6.48	0.0250	92	7.26	0.0107	92	6.67	0.0271	65		
	$6e_1 \rightarrow 8e_1$												34		
A_1	$9a_1 \rightarrow 10a_1$										6.65	0.0313	33		
	$6e_1 \rightarrow 8e_1$												62		
E_1	$2e_2 \rightarrow 7e_1$	6.59	0.0782	94	6.76	0.0282	94	5.75	0.0001	98	5.72	$\ll 10^{-4}$	100		
A_1	$6e_1 \rightarrow 8e_1$	6.72	0.5551	50	6.75	0.5051	54	7.03	0.4786	0					
	$3e_2 \rightarrow 4e_2$			14			18			66					
	$6e_1 \rightarrow 7e_1$			14			12			12					
	$5e_1 \rightarrow 7e_1$			10			0			0					
A_1	$6e_1 \rightarrow 8e_1$	6.90	0.2662	40	6.92	0.2626	38				6.92	0.4135	0		
	$3e_2 \rightarrow 4e_2$			40			44						68		
	$6e_1 \rightarrow 7e_1$			12			0						12		
A_1	$4e_1 \rightarrow 7e_1$	7.00	0.0883	56	7.15	0.0552	54	6.20	0.3124	64	6.16	0.3521	60		
	$3e_2 \rightarrow 4e_2$			20			12			0			0		
	$5e_1 \rightarrow 7e_1$			0			12			22			24		
	$9a_1 \rightarrow 11a_1$			0			10			0			0		

[a] Molecular Orbital. [b] Oscillator strength. [c] Percentage of the corresponding electron configuration in the total density. [d] w=weak and s=strong.

identification of the IP by the HOMO eigenvalue is not reproduced by the LDA and B88P86 calculations. It is well known that whereas the HOMO eigenvalue should be equal for the exact functional to the IP of the molecule,[50] this is definitely far from true for standard GGA functionals. Though this subject was still under discussion,[51–53] Casida has indeed proven,[54] using the correlated optimized effective-potential model, that the HOMO eigenvalue should equal the IP for the exact functional. Furthermore, he has reconciled the fractional occupation method and the statistical average theory. The failure of standard functionals is to be related to the exchange-correlation potential tails, which are incorrect and then leading to too many weakly bounding states near the Fermi level. On the contrary, the LB94 and LRC potentials overcorrect the IP value. However, the estimate is substantially improved. Finally, it can be stressed that Slater's transition state[4] method (HOMO eigenvalue of a self-consistent calculation of the molecule after removing half an electron) gives a very accurate value for the IP.

2. Transition Energies. a. TD-DFRT Calculation Using the LDA Geometry. The experimental spectrum[48] exhibits two huge peaks at 4.43 and 6.20 eV and two small peaks, at least 100 times weaker than the previous one, located at 2.68 and 3.22 eV.

Before interpreting the results, one should make some comments on the correspondence between theoretical and experimental spectra (see Table 6). Concerning the low lying states, there is no ambiguity as we know experimentally that the two bands at 2.68 eV and 3.22 eV are weak and that they have the same intensity. This is exactly what is found in our calculations. On the contrary, the assignment of high-lying states is much more ambiguous. According to previous studies,[11,16,55] the mean deviation of the excitation energies amounts to about 0.4 to 0.6 eV using TD-DFRT. Furthermore, the relative intensities between experimental bands are quite well reproduced by the calculations.[16] We know from experiment that the ratio between the small and the strong peaks is at least 100. Considering that the first $^1A_1$ state is about 1000 times more intense than the two low lying states and that the deviation of the energy is about 0.4 eV, we assigned this peak to the exp. 4.43 eV band. For the last peak, there are two candidates: the fifth $^1E_1$ state and the third $^1A_1$ state. The latter state is about

2500 times more intense than the two small peaks, but the mean energy deviation is much greater than the one commonly admitted. On the contrary, the $^1E_1$ state is about 250 times more intense and the mean deviation is acceptable. Therefore, as a compromise between these criteria, the $^1E_1$ state is suggested to correspond to the exp. 6.20 eV band.

Results obtained with LDA//LDA, B88P86//LDA and LB94//LDA procedures (Table 6) compare reasonably with experiment, the mean deviation from experiment amounting to 0.47, 0.51, and 0.33 eV, respectively. On one hand, the two strong bands located at 4.43 and 6.20 eV are exceptionally well reproduced by the LB94 functional, the overestimation being negligible compared to that of LDA and BP86 functionals (which are about 0.20 eV too high). On the other hand, none of the functionals used in combination with the LDA geometry give a satisfactory estimate of the two small peaks. As a general trend, the energies of these peaks are overestimated by 0.6 to 0.8 eV. However, the splitting between the experimental peaks amounting to 0.53 eV is well reproduced by the calculations (from 0.4 to 0.5 eV depending on the functional). Furthermore, the relative intensities between the two pairs of weak and strong peaks are experimentally estimated to amount at least to 100. This is in good agreement with our calculations which predicts a rate of 100 to 1000.

At first sight, comparing the LDA//LDA and the B88P86//LDA procedures, it is not logical to use a gradient-corrected potential functional in conjunction with a geometry calculated with the VWN functional. Indeed, the gradient-corrected B88P86 functional always overestimates transition energies and gives even worse values than the LDA//LDA procedure. In general, transitions are increased by about 0.06 eV (i.e., 500 cm^{-1}) except for the $^1E_1$ excited states at 6.20 and 6.42 eV where both energies are identical for the two procedures. Furthermore, it is of interest to note that both oscillator strength and composition of the density of the excited state are also almost strictly identical for the LDA//LDA and the B88P86//LDA procedures.

It is also of interest to emphasize that, even for low-lying states, the use of the asymptotically well-behaved LB94 or LRC functionals improves the transition energies. Compared to the LDA//LDA results, the prediction of the peak at 4.43 eV is significantly improved with the LB94 potential leading to a discrepancy of only 0.03 eV with experiment. The LRC potential predicts exactly the experimental value. The peak emerging at 6.20 eV is also well described by the LB94//LDA or LRC//LDA procedures, the deviation from experiment being of the same order of magnitude (0.04 and 0.08 eV, respectively). On the contrary, the two small peaks are still poorly reproduced by both functionals, the relative error amounting to at least 0.6 eV. In all cases, LB94 and LRC excitations energies are too high. This is in agreement with the general trend that the LB94 slightly underestimates the mean polarizabilities of molecules.[55]

Finally, the optical spectrum calculated with the LB94 functional shows substantial differences compared to that of LDA or B88P86 functionals as it exhibits numerous inversions in the ordering of the peaks. Therefore it becomes sometimes difficult to assign the corresponding peaks between the two spectra. As examples, the transition $^1E_1(6e_1 \rightarrow 10a_1) \leftarrow {}^1A_1$ at 5.90 eV is upshifted by 0.51 eV, whereas the transition $^1E_1(2e_2 \rightarrow 7e_1) \leftarrow {}^1A_1$ at 6.59 eV is downshifted by 0.84 eV. This behavior has already been emphasized in the literature: the time-dependent local density approximation (TDLDA) exhibits some inversion compared to the assignment proposed by the experimentalists. This is particularly true for states that meet one of the two criteria evidenced by Casida et al. in their work.[55] TDLDA exhibits some "fallen states" whether the excitation energy is close to the $-\epsilon_{HOMO}$ eigenvalue of the molecule or if the transition involves virtual molecular orbitals that are unbound (i.e., which have positive orbital energies). As an example, TDLDA gives the $B^3\Pi_g$ excited state of N_2 lying beneath the $A^3\Sigma_u$ state while the contrary is experimentally proven. In the case of the CpNiNO complex, one could probably consider the two states $|^1E_1> = 5.90$ eV and $|^1E_1> = 6.19$ eV as "fallen states" (the first one because the transition energy is close to the IP of the complex and the second one because the virtual orbitals $4e_2$ and $7e_1$ are very close to the Fermi level) if it was not in contradiction to what is found using the LRC potential. Actually, this potential leads roughly to the same excitation energy as the LDA and B88P86 ones for the first $^1E_1$ state (at 5.90 eV). There is little doubt, however, that the 6.19 eV state is a "fallen state" as LB94 and LRC results are in agreement within each other.

b. TD-DFRT Calculations Using GGA Geometries. On one hand, comparing the LDA//LDA and B88P86//B88P86 procedures (Tables 6 and 7), we can observe that the second one systematically lowers the transition energies. As we have seen in previous sections, LDA transitions are overestimated. Therefore, we can acertain that the use of B88P86 functional at the corresponding geometry improves the transition energies. The mean deviation between experimental and calculated energies is almost twice as low from LDA//LDA (0.47 eV) to B88P86//B88P86 (0.26 eV) procedures. This trend is still valid between the B88P86//LDA and the B88P86//B88P86 procedures. Concerning the ordering of the states, their compositions in terms of determinants and the intensities of the bands, there is no significant difference between the LDA//LDA, B88P86//LDA, and B88P86//B88P86 procedures.

On the other hand, whereas the LB94 (or LRC) functional systematically improves the description of vertical excitations at LDA geometries (Table 6), this is not so straighforward using the B88P86 geometry (Table 7). Roughly speaking, the quality of the LB94//B88P86 and LRC//B88P86 procedures lies between the LDA//LDA and B88P86//B88P86 procedures, with a mean deviation amounting to 0.37 eV compared to experiment. The description of the lowest experimental peak (2.68 eV) is still improved using the well-behaved potentials. On the contrary, the peak at 3.54 eV (according to B88P86//B88P86) is not significantly modified. Finally, for the two intense peaks, the position of the bands are better predicted by the B88P86//B88P86 calculations than by the LB94//B88P86 or LRC//B88P86 calculations.

Finally, it is noteworthy that for both LDA and GGA geometries, the shift between the small peaks and the shift between the stronger peaks are well reproduced by all the functionals. However, one can notice a discrepancy between CpNiNO and small molecules studied elsewhere[55] for the behavior of traditional functionals and well-behaved potentials: according to previous studies, compared to experiment, LDA and B88P86 functionals systematically downshift the whole spectrum. This is never observed for CpNiNO. Furthermore, whereas LB94 and LRC functionals should correct the LDA and GGA behaviors by upshifting the spectrum, they mostly downshift the spectrum in the case of CpNiNO. Anyway, the final results are in agreement with previous studies, namely the well-behaved functionals improve excitation energies.

Concerning the oscillator strength, we can notice that regardless of the peak considered, the intensities of the bands do not depend strongly on the functional used, as far as the VWN and

TABLE 7: Optical Absorption of the CpNiNO Complex at the GGA Geometry

		B88P86//B88P86			LB94//B88P86			LRC//B88P86			exp[48]	
symmetry	M. O.[a]	energy (eV)	f (a.u.)[b]	%[c]	energy (eV)	f (a.u.)[b]	%[c]	energy (eV)	f (a.u.)[b]	%[c]	energy (eV)	intensity[d]
E_1	$9a_1 \rightarrow 7e_1$	3.22	0.0004	63	3.08	0.0004	87	3.11	0.0002	81	2.68	w
	$3e_2 \rightarrow 7e_1$			36			7			9		
E_1	$9a_1 \rightarrow 7e_1$	3.54	0.0008	37	3.52	0.0004	13	3.48	0.0002	19	3.22	w
	$3e_2 \rightarrow 7e_1$			62			86			82		
A_1	$6e_1 \rightarrow 7e_1$	4.58	0.3739	58	4.24	0.4128	70	4.22	0.4152	64	4.43	s
	$5e_1 \rightarrow 7e_1$			34			24			24		
E_1	$6e_1 \rightarrow 10a_1$	5.88	0.0132	99	6.42	0.0012	94	5.85	0.0009	100		
E_1	$3e_2 \rightarrow 4e_3$	5.98	0.0070	86	6.41	0.0166	78	6.28	0.0009	88		
	$8a_2 \rightarrow 7e_2$			0			10			0		
E_1	$6e_1 \rightarrow 4e_2$	6.25	0.1328	70	5.97	0.0364	54	5.95	0.0283	52	6.20	s
	$3e_2 \rightarrow 4e_2$			14			44			0		
	$8a_2 \rightarrow 7e_2$			14			44			44		
A_1	$9a_1 \rightarrow 10a_1$	6.39	0.0553	87	7.22	0.0009	86	6.65	0.0971	82		
E_1	$2e_2 \rightarrow 7e_1$	6.54	0.0048	98	5.54	$\ll 10^{-4}$	100	5.51	$\ll 10^{-4}$	100		
A_1	$3e_1 \rightarrow 4e_2$	6.54	0.6859	62	6.74	0.4771	70	6.59	0.3478	36		
	$6e_1 \rightarrow 7e_1$			20			12			0		
	$5e_1 \rightarrow 7e_1$			0			10			0		
	$6e_1 \rightarrow 8e_1$			0			0			26		
	$9a_1 \rightarrow 10a_1$			0			0			17		
A_1	$6e_1 \rightarrow 8e_1$	6.81	0.0138	72	7.27	0.0348	86	6.68	0.0477	64		
	$3e_2 \rightarrow 4e_2$			10			0			24		
	$9a_1 \rightarrow 10a_1$			0			12			0		
A_1	$4e_1 \rightarrow 7e_1$	6.97	0.0573	56	6.00	0.2482	72	5.96	0.2790	64		
	$6e_1 \rightarrow 8e_1$			20			0			0		
	$5e_1 \rightarrow 7e_1$			0			18			18		

[a] Molecular orbital. [b] Oscillator strength. [c] Percentage of the corresponding electron configuration in the total density. [d] w=weak and s=strong.

B88P86 functionals are concerned. On the contrary, the LB94 functional exhibits some differences. As an example, the intensity of the transition $^1E_1(2e_2 \rightarrow 7e_1) \leftarrow {}^1A_1$ is almost zero according to LB94 or LRC calculations, whereas it is about 300 times higher with the B88P86 functional.

D. Conclusion on Metallocenes

As far as the $FeCp_2$ and the $RuCp_2$ complexes are concerned, the LDA//LDA procedure predicts excitation energies with the best accuracy. Gradient corrected geometries lead, most of the time, to excited states that are too low. In this case, the maximum error amounts to 0.7 eV. On the contrary, for the CpNiNO complex, the B88P86 functional improves the description of both the geometrical parameters and the excited states.

VI. General Conclusion

Results obtained for metal oxide complexes are in general satisfactory, except for the MnO_4^- compound, which is still an "enfant terrible" in DFT. The behavior of TD-DFT has shown to be a disaster for CrF_6, at least for the GGA geometries. Further studies should be undertaken on this class of metal complexes: are those results related to a lack of accuracy in the description of electron pairs with the exchange potential we used? Concerning metallocenes ($FeCp_2$ and $RuCp_2$), calculations compare well to experiment using the LDA geometry, whereas, for the CpNiNO complex, results are better at the GGA geometry.

In this article we show that, in general, the VWN geometries are satisfactory. As a consequence, the prediction of vertical excitations is accurate for low-lying states as long as one uses a functional with correct asymptotic behavior, such as the LB94 or LRC functionals. It is noteworthy that the ΔSCF method and the LB94//LDA and LRC//LDA procedures give roughly similar results.

At the LDA geometry, the gradient corrected functional B88P86 systematically increases the transition energies as compared to LDA ones. From B88P86 to LB94 and LRC, this trend is also observed as far as low-lying states are considered. On the contrary, at the B88P86 or PW91 geometries, transition energies are always lower than the transitions obtained with the LDA//LDA procedure.

As previously mentioned by Casida and co-workers[55] in a study bearing on small organic molecules, the relative ordering of the states is not changed between VWN and B88P86 calculations. On the contrary, the well-behaved functionals yield an important reordering of high lying states.

Contrary to previous work involving biological molecules,[55] where the LB94 functional yields better results than conventional functionals for high-lying states, we have shown that, at the GGA geometry, the B88P86 is the best functional for the CpNiNO complex. However, as far as we know, no experimental data are available on states higher than 6.20 eV for CpNiNO.

Finally, the hybrid B3LYP functional is not completely satisfactory as compared to pure LDA or GGA density functionals. In general, the B3LYP functional is less accurate than the B88P86 one and sometimes yields transition energies for low-lying states that are dramatically too low.

Acknowledgment. The authors thank Dr. Mark Casida for stimulating discussions. This work is supported by the Swiss National Science Foundation.

References and Notes

(1) Slater, J. C. *Phys. Rev.* **1951**, *81*, 385.
(2) Hohenberg, P.; Kohn, W. *Phys. Rev. A* **1964**, *136*, 864.
(3) Kohn, W.; Sham, L. J. *Phys. Rev. A* **1965**, *140*, 1133.
(4) Slater, J. C. *Quantum Theory of Molecules and Solids*; McGraw-Hill: New York, 1974.
(5) Ziegler, T.; Rauk, A.; Baerends, E. J. *Theor. Chim. Acta* **1977**, *43*, 261.
(6) Daul, C. *Int. J. Quantum Chem.* **1994**, *52*, 867.

(7) Casida, M. E. *Time-Dependent Density Functional Response Theory for Molecules*; Chong, D. P., Ed.; World Scientific: Singapore, Recent Advances in Density functional Methods, 1995; 155−192.
(8) Casida, M. E. *Time-Dependent Density Functional Response Theory of Molecular Systems: Theory, Computional Methods and Functionals*, Seminario, J. M., Ed.; Elsevier Science B. V.: Amsterdam, Theoretical and Computational Chemistry, 1995; 391−439.
(9) Gross, E. K. U.; Dobson, J. F.; Petersilka, M. *Density Functional Theory of Time-Dependent Phenomena*; Nalewalski, R. F., Ed.; Springer: Berlin, Topics in Current Chemistry, 1996; 81−172.
(10) van Leeuwen, R. *Phys. Rev. Lett.* **1998**, *80*, 1290.
(11) Jamorski, C.; Casida, M. E.; Salahub, D. R. *J. Chem. Phys.* **1996**, *104*(13), 5134.
(12) Handy, N. C.; Tozer, D. J. *J. Comput. Chem.* **1999**, *20*, 106.
(13) Osinga, V. P.; van Gisbergen, S. J. A.; Snijders, J. G.; Baerends, E. J. *J. Chem. Phys.* **1997**, *106*, 5091.
(14) Ioannou, A. G.; Amos, R. D. *Chem. Phys. Lett.* **1997**, *279*, 17.
(15) Nguyen, K. A.; Day, P. N.; Pachter, R. *J. Chem. Phys.* **1999**, *110*, 9135.
(16) van Gisbergen, S. J. A.; Goeneveld, J. A.; Rosa, A.; Snijders, J. G.; Baerends, E. J. *J. Phys. Chem.* **1999**, *103*, 6835.
(17) Baerends, E. J.; Bérces, A.; Bo, C.; Boerrigter, P. M.; Cavallo, L.; Deng, L.; Dickson, R. M.; Ellis, D. E.; Fan, L.; Fischer, T. H.; Fonseca Guerra, C.; van Gisbergen, S. J. A.; Groeneveld, J. A.; Gritsenko, O. V.; Harris, F. E.; van den Hoek, P.; Jacobsen, H.; van Kessel, G.; Kootstra, F.; van Lenthe, E.; Osinga, V. P.; Philipsen, P. H. T.; Post, D.; Pye, C. C.; Ravenek, W.; Ros, P.; Schipper, P. R. T.; Schreckenbach, G.; Snijders, J. G.; Sola, M.; Swerhone, D.; te Velde, G.; Vernooijs, P.; Versluis, L.; Visser, O.; van Wezenbeek, E.; Wiesenekker, G.; Wolff, S. K.; Woo, T. K.; Ziegler, T. ADF1999.
(18) Fonseca Guerra, C.; Snijders, J. G.; te Velde, G.; Baerends, E. J. *Theor. Chem. Acc.* **1998**, *99*, 391.
(19) van Gisbergen, S. J. A.; Snijders, J. G.; Baerends, E. *J. Comput. Phys. Commun.* **1999**, *118*, 119.
(20) Vosko, S. H.; Wilk, L.; Nusair, M. *Can. J. Phys.* **1980**, *58*, 1200.
(21) Becke, A. D. *Phys. Rev. A* **1988**, *38*, 3098.
(22) Perdew, J. P. *Phys. Rev. B* **1986**, *33*, 8822.
(23) van Leeuwen, R.; Baerends, E. J. *Phys. Rev. A* **1994**, *49*, 2421.
(24) Lembarki, A.; Rogemond, F.; Chermette, H. *Phys. Rev. A* **1995**, *52*, 3704.
(25) Perdew, J. P. *Electronic Structure of Solids '91*, P. Ziesche, H. Eschrig; Akademie Verlag: Berlin, 1991, 1994.
(26) Becke, A. D. *J. Chem. Phys.* **1993**, *98*, 5648.
(27) Gaussian98(Revision A.7), Frisch, M. J.; Trucks, G. W.; Schlegel, H. B.; Scuseria, G. E.; Robb, M. A.; Cheeseman, J. R.; Zakrzewski, V. G.; Montgomery, J. A.; Stratmann, R. E.; Burant, J. C.; Dapprich, S.; Millam, J. M.; Daniels, A. D.; Kudin, K. N.; Strain, M. C.; Farkas, O.; Tomasi, J.; Barone, V.; Cossi, M.; Cammi, R.; Mennucci, B.; Pomelli, C.; Adamo, C.; Clifford, S.; Ochterski, J.; Petersson, G. A.; Ayala, P. Y.; Cui, Q.; Morokuma, K.; Malick, D. K.; Rabuck, A. D.; Raghavachari, K.; Foresman, J. B.; Cioslowski, J.; Ortiz, J. V.; Stefanov, B. B.; Liu, G.; Liashenko, A.; Piskorz, P.; Komaromi, I.; Gomperts, R.; Martin, R. L.; Fox, D. J.; Keith, T.; Al-Laham, M. A.; Peng, C. Y.; Nanayakkara, A.; Gonzalez, C.; Challacombe, M.; Gill, P. M. W.; Johnson, B. G.; Chen, W.; Wong, M. W.; Andres, J. L.; Head-Gordon, M.; Replogle, E. S.; Pople, J. A. Gaussian, Inc., Pittsburgh, PA 1998.
(28) Dunning, T. H., Jr.; Hay, P. J. *Modern Theoretical Chemistry*; Schaefer, H. F., III; Plenum: New York, 1976.
(29) Wolfsberg, M.; Helmholz, L. J. *Chem. Phys.* **1952**, *20*, 837.
(30) Stückl, A. C.; Daul, C.; Güdel, H. U. *Int. J. Quantum Chem.* **1997**, *61*, 579.
(31) Johnson, I. W.; McGlynn, S. P. *Chem. Phys. Lett.* **1970**, *7*, 618.
(32) Tozer, D. J.; Handy, N. C. *J. Chem. Phys.* **1998**, *109*, 10180.
(33) Tozer, D. J.; Amos, R. D.; Handy, N. C.; Roos, B. O.; Serrano-Andrés, L. *Mol. Phys.* **1999**, *97*, 859.
(34) Gritsenko, O. V.; Schipper, P. R. T.; Baerends, E. J. *Chem. Phys. Lett.* **1999**, *302*, 199.
(35) Casida, M. E.; Casida, K. C.; Salahub, D. R. *Int. J. Quantum Chem.* **1996**, *70*, 933.
(36) Holt, S. L.; Ballhausen, C. J. *Theor. Chim. Acta* **1967**, *7*, 313.
(37) Kálmán, A. *J. Chem. Soc.* 1971, A, 1857.
(38) Palenik, G. J. *Inorg. Chem.* **1967**, *6*, 503.
(39) Robbins, D. J.; Day, P. *Mol. Phys.* **1977**, *34*, 893.
(40) Goursot, A.; Daul, C. in *NATO ASI Series, Vol. C176*, A. Veillard, Ed. (D. Reidel: Dordrecht, 1986), pp 199−208).
(41) Dickson, R. M.; Ziegler, T. *Int. J. Quantum Chem.* **1996**, *58*, 681.
(42) Ortner, M. H. *J. Chem. Phys.* **1961**, *34*, 556.
(43) Muller, A.; Diemann, E.; Jorgensen, C. K. *Struct. Bond.* **1973**, *14*, 23.
(44) Hope, E. G.; Jones, P. J.; Levason, W.; Ogden, J. S.; Tajok, M.; Turff, J. W. *J. Chem. Soc., Dalton Trans.*, **1985**, 1448.
(45) Sohn, Y. S.; Hendrickson, D. N.; Gray, H. B. *J. Am. Chem. Soc.* **1971**, *93*, 3603.
(46) Daul, C.; Güdel, H.-U.; Weber, J. *J. Chem. Phys.* **1993**, *98*, 4023.
(47) Seiler, P.; Dunitz, J. D. *Acta Crystallogr.* **1980**, *B 36*, 2946.
(48) Chen, L. X.; Bowman, M. K.; Wang, Z.; Montano, P. A.; Norris, J. R. *J. Phys. Chem.* **1994**, *98*, 9457.
(49) Field, C. N.; Green, J. C.; Mayer, M.; Nastuzov, V. A.; Rösch, N.; Siggel, M. R. F. *Inorg. Chem.* **1996**, *35*, 2504.
(50) Levy, M.; Perdew, J. P.; Parr, R. G.; Balduz, J. L. *Phys. Rev. Lett.* **1982**, *49*, 1691.
(51) Kleinman, L. *Phys. Rev. B* **1997**, *56*, 12042.
(52) Perdew, J. P. *Phys. Rev. B* **1997**, *56*, 16021.
(53) Kleinman, L. *Phys. Rev. B* **1997**, *56*, 16029.
(54) Casida, M. E. *Phys. Rev A* **1999**, *59*, 4694.
(55) Casida, M. E.; Jamorski, C.; Casida, K. C.; Salahub, D. R. *J. Chem. Phys.* **1998**, *108*, 4439.
(56) Haaland, A. *Acc. Chem. Res.* **1979**, *12*, 415.